2010

Variable-wavelength frequency-domain terahertz ellipsometry

Tino Hofmann
University of Nebraska-Lincoln, thofmann4@unl.edu

C. M. Herzinger
J.A. Woollam Co.

A. Boosalis
University of Nebraska-Lincoln

T. E. Tiwald
J.A. Woollam Co. Inc.

John A. Woollam
University of Nebraska-Lincoln, jwoollam1@unl.edu

See next page for additional authors

Variable-wavelength frequency-domain terahertz ellipsometry

T. Hofmann,[1,a)] C. M. Herzinger,[2] A. Boosalis,[1] T. E. Tiwald,[2] J. A. Woollam,[2] and M. Schubert[1]
[1]*Department of Electrical Engineering and Nebraska Center for Materials and Nanoscience, University of Nebraska–Lincoln, Nebraska 68588-0511, USA*
[2]*J.A. Woollam Co. Inc., 645 M Street, Suite 102 Lincoln, Nebraska 68508, USA*

(Received 25 November 2009; accepted 2 January 2010; published online 2 February 2010)

We report an experimental setup for wavelength-tunable frequency-domain ellipsometric measurements in the terahertz spectral range from 0.2 to 1.5 THz employing a desktop-based backward wave oscillator source. The instrument allows for variable angles of incidence between 30° and 90° and operates in a polarizer-sample-rotating analyzer scheme. The backward wave oscillator source has a tunable base frequency of 107–177 GHz and is augmented with a set of Schottky diode frequency multipliers in order to extend the spectral range to 1.5 THz. We use an odd-bounce image rotation system in combination with a wire grid polarizer to prepare the input polarization state. A highly phosphorous-doped Si substrate serves as a first sample model system. We show that the ellipsometric data obtained with our novel terahertz ellipsometer can be well described within the classical Drude model, which at the same time is in perfect agreement with midinfrared ellipsometry data obtained from the same sample for comparison. The analysis of the terahertz ellipsometric data of a low phosphorous-doped *n*-type Si substrate demonstrates that ellipsometry in the terahertz spectral range allows the determination of free charge-carrier properties for electron concentrations as low as 8×10^{14} cm^{-3}. © *2010 American Institute of Physics.*
[doi:10.1063/1.3297902]

I. INTRODUCTION

Electromagnetic radiation at terahertz frequencies offers unique properties that are of great interest for basic research, communication systems, and security applications.[1–3] This has spurred growing interest in terahertz source and detector technologies[4–9] for use in novel sensing and communication systems. To facilitate continued developments, measurement tools and techniques to characterize terahertz optical properties of materials, components, and systems are consequently needed.[10,11] In the same way as for infrared (IR)-visible-UV optics, accurate terahertz material optical constants will be needed for designing components, verifying those designs, and for developing and controlling manufacturing processes. This will be most directly achieved by a measurement technique that uses the frequencies of actual interest. Basic scientific research is another reason that the accurate complex optical properties of materials at terahertz frequencies are of interest.[9] There exists a wealth of fascinating excitation mechanisms with eigenfrequencies in the terahertz domain in condensed and soft matter such as spin transitions, collective modes of biological molecules, local free charge-carrier oscillations, dynamic motion of magnetic domains, ferroelectric domains, or collective charge phenomena, as examples. Measurement of the complex optical properties at terahertz frequencies may further allow exploration of novel physical phenomena as observed in artificially structured metamaterials.[12–14]

Ellipsometry is established as the preeminent method used to precisely determine the optical properties for wavelengths from the far IR (FIR) through the vacuum UV.[15,16] Ellipsometers are employed in a wide variety of applied and basic research fields because they can produce highly accurate, nondestructive measurements suitable for quantitative analysis. Ellipsometry in traditional FIR-visible-UV spectral ranges utilizes essentially steady-state illumination and modulation frequencies much lower than the illuminating light optical frequency. The key element of ellipsometry, as compared to other optical measurement techniques, is that measurements are made synchronously with the modulation of the optical polarization state. At the most basic level, one polarization state is measured relative to another polarization state. Ellipsometry is therefore much less sensitive to nonidealities of the measurement system than intensity-normalized measurement techniques.[17–20] Ellipsometry in the terahertz frequency domain, however, is still in its infancy and experimental reports are scarce.[21–26]

Nagashima and Hangyo[21] demonstrated the first ellipsometry setup operating in the terahertz frequency range. By augmenting a terahertz time-domain spectrometer by fixed polarizers the *p* and *s*-polarized reflectivities and thereby the complex optical constants of a moderately phosphorous-doped *n*-type silicon substrate were determined. A similar approach was used later by[22] in magneto-optical Kerr effect measurements on InAs. In two earlier publications we presented the first frequency-domain terahertz magneto-optic generalized ellipsometry experiments using highly brilliant terahertz synchrotron radiation for the determination of free charge-carrier properties in ZnMnSe/GaAs and highly oriented pyrolytic graphite.[23,24] Recently, we employed the

a)Electronic mail: thofmann@engr.unl.edu.

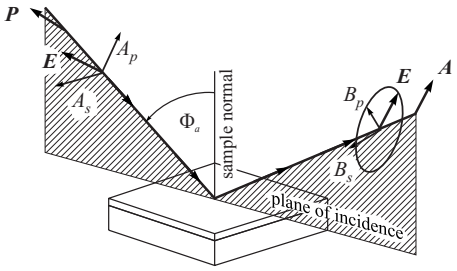

FIG. 1. Definition of the plane of incidence (p plane) and the incidence angle Φ_a through the wave vectors of the incident and emerging (reflection setup) plane waves. A_p, A_s, B_p, and B_s denote the complex amplitudes of the p and s modes before and after reflection, respectively. P and A are the azimuth angles of the linear polarizer as used in the standard arrangement of rotating-analyzer ellipsometer.

frequency-domain terahertz ellipsometer setup which is described here in detail for the determination of free charge-carrier diffusion profiles in silicon.[25]

Here we describe a novel wavelength-tunable frequency-domain ellipsometry setup operating in the spectral range from 0.2 to 1.5 THz. In order to illustrate our terahertz ellipsometry setup, describe the measurement algorithm, and discuss the data analysis procedures we have selected silicon substrates with different free charge-carrier properties as a simple model system. Measurements in the mid-IR (MIR) spectral range were augmented to cross reference the terahertz system using comparison in a simultaneous optical-model analysis.

II. THEORY

A. Ellipsometry

Ellipsometry determines the change in the polarization state of an electromagnetic plane wave upon interaction with a sample. This change is commonly cast into the complex-valued scalar ratio ρ relating two linearly independent complex amplitudes of the propagating eigenmodes of polarized electromagnetic plane waves before (A_ζ, A_ξ) and after $(B_{\zeta'}, B_{\xi'})$ sample interaction (Fig. 1 depicts the reflection setup, the transmission case is alike),[27–29]

$$\rho = \left(\frac{B_{\zeta'}}{B_{\xi'}}\right) \Big/ \left(\frac{A_\zeta}{A_\xi}\right) = \tan\Psi \exp(i\Delta). \tag{1}$$

The result of an ellipsometry measurement is often presented by real-valued parameters Ψ and Δ, where now $\tan\Psi$ is defined as the absolute value of the complex ratio, and Δ denotes the relative phase change in the p and s components of the electric field vector in Eq. (1). Measurement of the complex ratio ρ can be addressed within different presentations of the electromagnetic plane wave response.[30] Convenient are the Stokes and Jones vector descriptions. While the Jones approach sufficiently frames the required extension for nondepolarizing samples, the Stokes formalism including Mueller matrices must be invoked for cases when either sample or the experimental setup cause partially depolarized light. The Jones vector is the usual arrangement of electric field vector amplitudes transverse to propagation direction (suppressing time dependence explicitly and thereby ignoring partial depolarization implicitly). The Jones matrix then relates Jones vectors before and after sample interaction

$$\begin{pmatrix} B_p \\ B_s \end{pmatrix} = \begin{pmatrix} j_{pp} & j_{sp} \\ j_{ps} & j_{ss} \end{pmatrix} \begin{pmatrix} A_p \\ A_s \end{pmatrix}. \tag{2}$$

Herein, case of either reflection or transmission is addressed as usual, remaining with the linear $p-s$ polarization system, while changes to $(j_{\zeta\xi'})$ will occur accordingly if conversion is done to other than $p-s$ presentation of fields before and/or after sample interaction. Notably, off-diagonal elements are nonzero for optical systems that convert p into s waves and vice versa. Owing to the artificial construction of the Jones vector, which cannot be directly related to physically observable quantities, model assumption has to be implemented in order to connect measurement with the ellipsometric parameters. An alternative description provides the Stokes vector formalism, where real-valued matrix elements connect the Stokes parameters of the electromagnetic plane waves before and after sample interaction, and which can, in principle, be directly measured because the linearly independent Stokes vector elements are well-defined, physically observable quantities. For the $p-s$ system: $S_0=I_p+I_s$, $S_1=I_p-I_s$, $S_2=I_{45}-I_{-45}$, $S_3=I_{\sigma+}-I_{\sigma-}$, where I_p, I_s, I_{45}, I_{-45}, $I_{\sigma+}$, and $I_{\sigma-}$ denote the intensities for the p, s, $+45°$, $-45°$, right-handed, and left-handed circularly polarized light components, respectively.[29,31,32] Importantly, S_0 is proportional to the total intensity of the light beam, and the inequality $S_0 \geqslant \sqrt{S_1^2+S_2^2+S_3^2}$ gives a measure of the degree of polarization while the equality sign holds for total polarized light only. Arranging the Stokes parameters into a column vector, the real-valued 4×4 Mueller matrix defined thereby then describes the changes in each quantity upon interaction of the electromagnetic plane wave with an optical system,[33]

$$S_j^{\text{output}} = \sum_{i=0}^{3} M_{ji} S_i^{\text{input}}, (j = 0 \ldots 3). \tag{3}$$

The advantage of this concept is the ability to handle situations with partial polarization of the electromagnetic plane wave, particularly when caused by device components' imperfections.[29,31,34–37]

Two different concepts emerge from Eq. (1). The standard and the generalized ellipsometry situations, which differ by the dependence of ρ on A_ζ/A_ξ. The standard ellipsometry situation requires ρ to be independent of A_ζ/A_ξ, while the general case includes all deviations from this restriction. The field components are commonly given in terms of p and s polarized fields in Fig. 1, relating both $(A_\zeta, A_\xi)=(A_p, A_s)$ and $(B_{\zeta'}, B_{\xi'})=(B_p, B_s)$ to the plane of incidence.

B. Standard isotropic ellipsometry

For standard isotropic ellipsometry Ψ and Δ do not depend on the polarization state of the incident plane wave. Within the Jones presentation the normalization expression is

$$\rho = \frac{j_p}{j_s} = \tan\Psi \exp(i\Delta). \tag{4}$$

The complex value defined this way has a historical basis in null ellipsometry, but also a useful practical consideration in that Ψ remains bounded even when the magnitude of ρ

becomes infinite. Here j_p and j_s denote the p and s-polarized complex reflection ("$j_{p,s}$" = "$r_{p,s}$") or transmission coefficients ("$j_{p,s}$" = "$t_{p,s}$"). For the normalized Mueller matrix approach—a nondepolarizing system taken as example—an one-to-one relation exists between matrices **j** and **M**.[29,38] If the sample is also isotropic, then $M_{11}=M_{22}=1$, $M_{12}=M_{21}=-\cos 2\Psi$, $M_{33}=M_{44}=\sin 2\Psi \cos \Delta$, $M_{34}=-M_{43}=\sin 2\Psi \sin \Delta$, and $M_{ij}=0$ otherwise, with the constraint $M_{11}^2+M_{33}^2+M_{34}^2=1$ (Ref. 36) and

$$\rho = \frac{M_{33} + iM_{34}}{1 - M_{12}}. \tag{5}$$

C. Generalized ellipsometry

By definition, in the nondepolarizing generalized ellipsometry situation Ψ and Δ can be generalized to define three ratios involving Jones matrix elements. This concept is valid within both the normalized Mueller matrix as well as the normalized Jones matrix formalism. Within the Jones presentation generic expressions for the generalized ellipsometry parameters are Ψ_{ij}, Δ_{ij} ("J,j" = "T,t" or "R,r"),[39]

$$\frac{j_{pp}}{j_{ss}} = \tan \Psi_{pp} \exp(i\Delta_{pp}),$$

$$\frac{j_{ps}}{j_{pp}} = \tan \Psi_{ps} \exp(i\Delta_{ps}), \tag{6}$$

$$\frac{j_{sp}}{j_{ss}} = \tan \Psi_{sp} \exp(i\Delta_{sp}).$$

The real-valued quantities Ψ_{pp}, Ψ_{ps}, Ψ_{sp}, Δ_{pp}, Δ_{ps}, and Δ_{sp} comprise the generalized ellipsometry data presentation in the Jones formalism. The ratios involving off-diagonal elements are a convenient choice for rotating-analyzer systems because input polarizations of 0° and 90° isolate the two ratios. Each normalized Jones matrix corresponds to a nondepolarizing normalized Mueller matrix.[29] However, for the most complicated sample situation involving anisotropy and depolarization, the Jones formalism is not sufficient and the full generality of the Mueller matrix formalism is needed.

D. Data analysis

In many circumstances ellipsometric measured values are not of direct interest and a further data analysis is necessary to extract sample parameters of real interest, e.g., layer thicknesses, optical constants, etc. Data analysis requires nonlinear regression methods, where measured and calculated ellipsometry spectra are matched as close as possible by varying appropriate physical model parameters. The calculations require setup of models for geometry, layer structure, and polarizability properties of materials involved in the sample of interest, and comprise the actual art in performing ellipsometry.

Due to the complexity of this subject, thorough discussion of this issue is beyond the scope of this paper, and referral is made to the literature. An excellent introduction can be found for instance in the chapter by Jellison in Ref. 28.

E. Terahertz dielectric function model

In principle, the samples' frequency-dependent dielectrical properties can be directly recovered from the measured ellipsometric data. The disadvantage of this model-independent wavelength-by-wavelength fit approach is that measurement noise becomes part of the extracted optical constants. The use of parameterized functions, i.e., using a physical model for ε provides most direct connection between measured and physical parameters of interest, and prevents wavelength-by-wavelength measurement noise from becoming part of the extracted optical constants. Details about parametric model approaches and use of multiple-sample-regression techniques are given in Refs. 40 and 41.

The parameterized model dielectric function in the terahertz and IR spectral range must correctly render the contributions from polar excitations $\varepsilon^{\mathrm{L}}(\omega)$ and free charge carriers $\varepsilon^{\mathrm{FC}}(\omega)$.[15] In particular, the free charge-carrier contributions can be described by the classical Drude approach[15,42]

$$\varepsilon^{\mathrm{FC}}(\omega) = \varepsilon_\infty - \frac{Nq^2}{\tilde{\varepsilon}_0 m(\omega^2 + i\omega/\tau)}, \tag{7}$$

where N is the free charge-carrier concentration, q denotes the charge, τ is the average energy-independent scattering time, and $\tilde{\varepsilon}_0$ is the vacuum permittivity. The dc conductivity $\sigma_{\mathrm{dc}}=qN\mu$ is related to the screened plasma frequency ω_p by $\sigma_{\mathrm{dc}}=\varepsilon_\infty \tilde{\varepsilon}_0 \omega_p^2 \tau$, where $\omega_p^2=Nq^2/(\varepsilon_\infty \tilde{\varepsilon}_0 m)$ and μ is the mobility given by $\mu=q\tau/m$. The high frequency dielectric constant and the effective mass of the free charge carriers is denoted by ε_∞ and m, respectively.

III. EXPERIMENTAL SETUP

The instrument presented here operates in the polarizer-sample-rotating analyzer arrangement[16] and permits ellipsometric measurements in the spectral range from 0.2 to 1.5 THz. The experimental setup is based on a θ-2θ high precision goniometer which allows for measurements at angles of incidence Φ_a from 30° to 90°. In some cases, variable angle spectroscopic ellipsometry provides additional independent information of the sample system. However, in all cases the inclusion of data at more than one angle of incidence provides internal self-consistency checks for the data analysis and also tends to balance available sensitivity to sample parameters which can change with angle of incidence.

A sketch of the experimental setup is given in Fig. 2. A backward wave oscillator (BWO) is employed as the radiation source. The nearly linearly polarized light emitted from the BWO is collimated by a Picarin lens (L). A variable odd-bounce polarization rotation system (PR) (Ref. 43) is used in combination with a polyethylene substrate, wire-grid polarizer (P) to control the incident polarization state. The mirrors M1–M3 steer the beam and focus the radiation to the sample stage (S) of a high-precision goniometer (HG). A continuously (f=.45 Hz) rotating polyethylene substrate wire grid polarizer is used as the polarization state analyzer (A). The terahertz radiation reflected from the sample is focused (M4) on Golay cell (GC) which serves as detector. The beam is modulated by an optical chopper (C) at f =12.6 Hz to match the frequency response of the Golay cell.

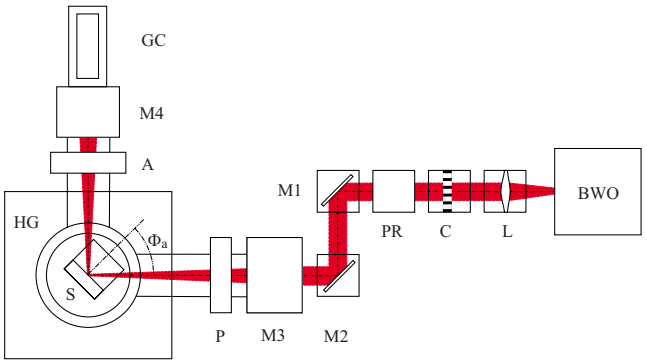

FIG. 2. (Color online) Beam path of the terahertz ellipsometer employed for the spectral range from 0.2 to 1.5 THz. The system is composed of a BWO source, the polarization control elements [variable odd-bounce image rotation system (PR), a wire grid polarizer (p), and a rotating analyzer (a)], the beam steering and focusing elements [Picarin lens (L), mirrors M1–M4], the detector (GC), the high-precision θ-2θ goniometer (HG) with the sample stage (S), and the optical chopper (C).

The BWO tube used here emits nearly linearly polarized light with a very narrow bandwidth of approximately 2 MHz and a very high output power of 0.1–0.01 W in the frequency range from 107 to 177 GHz. The high output power in this base band is converted to higher frequency bands using a set of planar GaAs Schottky diode frequency multipliers. The spectral ranges from 220 to 350 GHz and from 330 to 525 GHz are covered using a single frequency doubler (D) and a frequency tripler (T). For the spectral ranges from 650 to 1040 and 980–1580 GHz two-stage frequency multiplier chains, a doubler+triper (DT) and a tripler+tripler (TT) were used. The output power of the BWO as a function of the frequency measured in straight-through configuration without polarizing elements in the beam path is shown in Fig. 3.

For cross referencing measurements, a commercial MIR Fourier transform-based ellipsometer was used in the range from 9 to 50 THz (300–1700 cm^{-1}). The instrument operates in a polarizer-sample-rotating compensator-analyzer

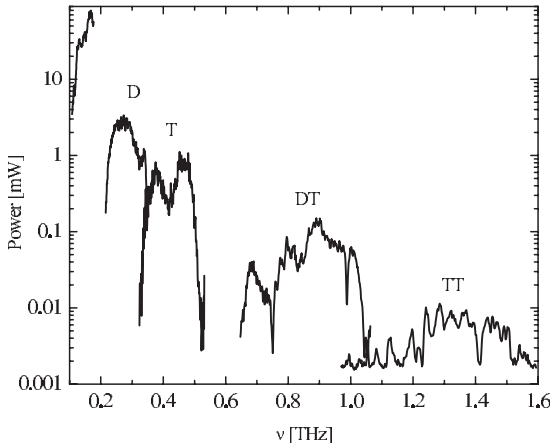

FIG. 3. Output power of the BWO as a function of the frequency ν determined in a straight-through configuration. The base resonator that covers the range from 107 to 177 GHz is augmented with GaAs Schottky diode multipliers: a frequency doubler (d), a frequency tripler (t), and two multiplier chains composed of: frequency doubler+tripler (DT) and frequency tripler +tripler (TT).

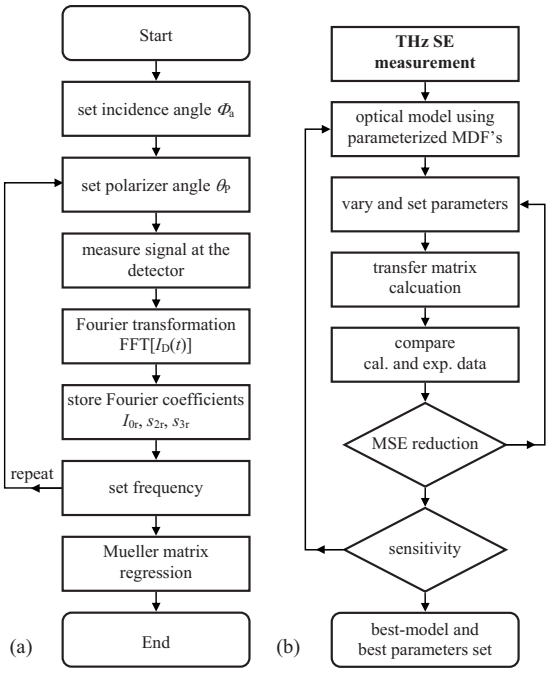

FIG. 4. Flowchart (a) of the algorithm employed for the terahertz ellipsometry measurement using the BWO source and the polarizer-sample-rotating-analyzer scheme. The flowchart to obtain the best-model parameters during the analysis of the experimental terahertz ellipsometry data is shown in (b).

arrangement[16] and is equipped with a SiC globar as a radiation source and a deuterated triglycine sulfate IR detector.

A. Data acquisition and analysis procedures

The ellipsometry data acquisition was performed as shown in Fig. 4. For the underlying equation describing the optical throughput of a rotating-analyzer ellipsometer system, the Stokes vector of the light beam at the Golay cell detector (GC) shown in Fig. 2 is determined by the product of the Mueller matrices of polarizer $\boldsymbol{M}_P$, sample $\boldsymbol{M}$, and analyzer $\boldsymbol{M}_A$ (Ref. 28) is given by

$$I_D \boldsymbol{s}_D = \boldsymbol{R}(-\theta_A)\boldsymbol{M}_A\boldsymbol{R}(\theta_A)\boldsymbol{M}\boldsymbol{R}(-\theta_P)\boldsymbol{M}_P\boldsymbol{R}(\theta_P)I_S\boldsymbol{s}_S. \quad (8)$$

The normalized Stokes vectors and the irradiance of the source [detector: Golay cell (GC) in Fig. 2] are denoted by $I_S(I_D)$ and $\boldsymbol{s}_S(\boldsymbol{s}_D)$, respectively. Analyzer and polarizer rotations are described by the rotation matrices $\boldsymbol{R}(\theta_j)$, with the angles $\theta_j(j=\text{“}A\text{”},\text{“}P\text{”})$.[24] The underlying equation describing the collected intensity can be expanded into a Fourier series[17,18]

$$I_D(\theta_A) = \frac{I_{0r}}{2}\{1 + s_{1r}\cos[2\theta_A(t)] + s_{2r}\sin[2\theta_A(t)]\}, \quad (9)$$

where $\boldsymbol{S}_r = I_{0r}\boldsymbol{s}_r = I_{0r}(1, S_{1r}, S_{2r}, S_{3r})^T$. I_{0r} denotes the irradiance of the beam. The detected signal is subjected to a Fourier analysis synchronous with the rotating analyzer to obtain normalized Fourier coefficients at harmonics generated by the analyzer. The normalized Fourier coefficients obtained at one or more input polarizer settings are then subjected to a numerical inversion process to extract the sample parameters of interest (e.g., normalized Mueller matrix elements) from Eq. (8).

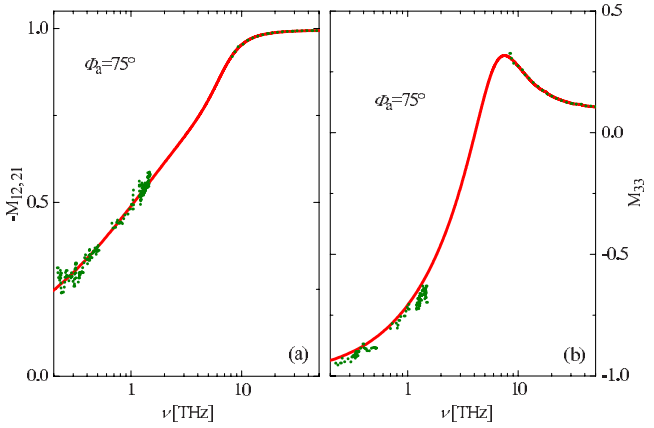

FIG. 5. (Color online) Experimental (dotted lines) and best-fit calculation (solid lines) $-M_{12,21}$ spectra (a) and M_{33} spectra (b) of the highly doped n-type Si substrate at $\Phi_a=75°$.

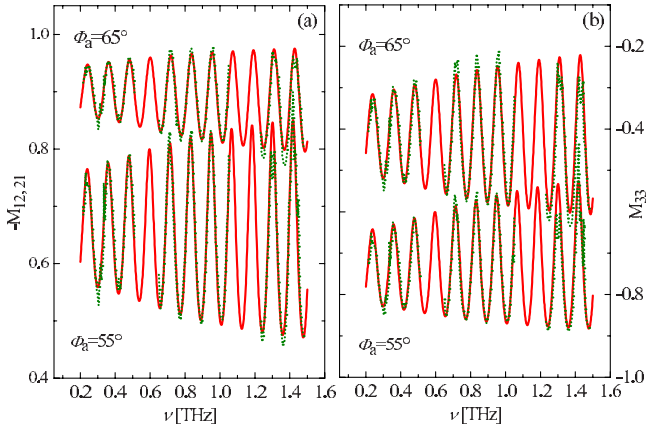

FIG. 6. (Color online) Experimental (dotted lines) and best-fit calculation (solid lines) $-M_{12,21}$ spectra (a) and M_{33} spectra (b) of the low doped n-type Si substrate at $\Phi_a=55°$ and 65°.

The system is calibrated using the regression calibration method for a rotating analyzer element ellipsometer described in Ref. 44. A set of normalized Fourier coefficients s_{1r} and s_{2r} is measured from an isotropic sample at a series of different input polarizer settings. An optical model which exactly describes the response of the ideal rotating analyzer system is then fit to the experimental data, using the Levenberg–Marquardt nonlinear regression algorithm, to determine the polarizer and analyzer azimuthal offsets simultaneously with the ellipsometric parameters for the isotropic sample. The advantage of this technique is that the calibration is based upon sample symmetry and does not require a specific known reference sample. Further details of the calibration data acquisition and analysis are described in Ref. 44.

B. Samples and measurements

As a demonstration two different bulklike phosphorous-doped n-type Si substrates were examined. The lower doped sample was double side polished with nominal resistivity of 5 Ω cm. The higher doped sample has a nominal resistivity of 0.02 Ω cm. Ellipsometric measurements were made assuming that the sample's normalized Mueller matrix was of the form described in Sec. II B.

IV. RESULTS AND DISCUSSION

The experimental and best-model calculated $-M_{12,21}$ spectra and M_{33} spectra of the highly phosphorous-doped n-type Si substrate obtained at an angle of incidence $\Phi_a=75°$ are depicted in Figs. 5(a) and 5(b), respectively. The data obtained from the terahertz ellipsometer setup and the commercial MIR ellipsometer are in excellent agreement with the calculations derived from a common model. A five phase model (ambient/native oxide/depletion region/highly doped Si/ambient) was employed for the simultaneous analysis of the terahertz and MIR data sets.

The dielectric function $\varepsilon(\omega)$ for doped silicon, governed by Eq. (7), dominates the features in the terahertz and IR spectral domains. However, in order to fully describe the experimental data throughout the entire terahertz-MIR region, the contributions of the oxide layer and the carrier depletion region at the substrate surface have to be included in the model. The dielectric function of the oxide consists of three Lorentz-like harmonic oscillators modeling the optically active Si–O rocking and stretching vibrations.[45] The oxide produces very subtle effects in the M_{33} spectra between 13 and 37 THz. The presence of the depletion layer is expressed as small offsets primarily in the MIR spectral region. The model analysis yields the thickness of the SiO_2 layer and the carrier depletion region of $d_{SiO2}=2.2\pm0.2$ nm and $d_{depl}=25\pm4$ nm, respectively. For the substrate resistivity and scattering time we obtain $\rho=0.023\pm0.001$ Ω cm and $\tau=26.9\pm0.5$ fs. Assuming an effective electron mass of $0.26m_0$ (Ref. 46) this corresponds to a free charge-carrier concentration $N=(1.51\pm0.01)\times10^{18}$ cm^{-3} and a mobility $\mu=182\pm3$ cm^2/V s.

Figure 6 shows the experimental and best-model calculated $-M_{12,21}$ spectra and M_{33} spectra obtained from the low phosphorous-doped Si substrate for two angles of incidence $\Phi_a=55°$ and 65°. The spectra are dominated by oscillations which originate from multiple internal reflections between the top and bottom silicon-air interface. It can be clearly seen that the amplitude of the Fabry–Pérot oscillations pattern is decreasing for lower frequencies. This can be attributed to free charge-carrier absorption in the sample. The effects of the surface depletion and the SiO_2 layer to the $-M_{12,21}$ spectra and M_{33} spectra are negligible and a simple three phase model (ambient/Si/ambient) was used for the data analysis consisting only of a doped Si layer. The best-model parameters obtained for the resistivity and scattering time are $\rho=5.01\pm0.16$ Ω cm and $\tau=239\pm9$ fs, respectively. This corresponds to a free charge-carrier concentration of $N=7.7\pm0.4\times10^{14}$ cm^{-3} and mobility of $\mu=1617\pm80$ cm^2/(V s) if an averaged electron effective mass of $0.26m_0$ (Ref. 46) is assumed. The plasma frequency is approximately 0.14 THz. For the thickness of the wafer we obtain 384.2 ± 0.1 μm which is highly consistent with the results obtained from the IR spectral range which are not shown here for brevity.

The real ε_1 and imaginary ε_2 part of the spectroscopic dielectric values for the doped Si were also extracted on a

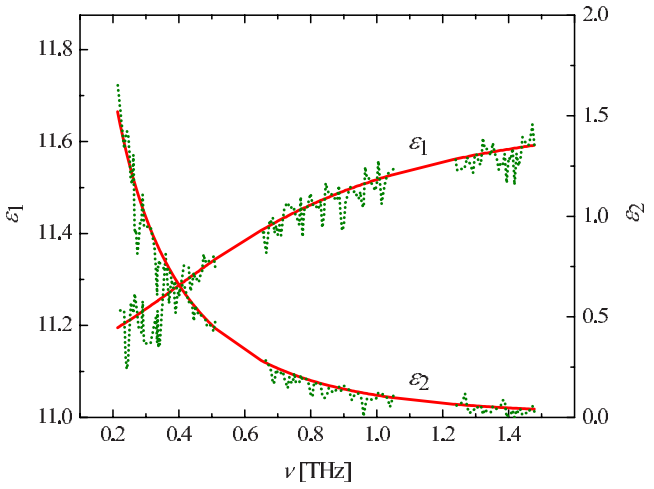

FIG. 7. (Color online) Wavelength-by-wavelength extracted (dotted lines) and Drude model calculated real (ε_1) and imaginary (ε_2) part of the dielectric function of the low phosphorous-doped *n*-type silicon substrate.

model free wavelength-by-wavelength basis (dotted lines) and are compared with the previous determined Drude functional model (solid lines) in Fig. 7. The wavelength-by-wavelength extracted data are in excellent agreement with the Drude model calculated data and show the typical increase in ε_2 for lower frequencies.

V. SUMMARY

In summary, we have successfully demonstrated a novel spectroscopic ellipsometry setup for measurements in the range from 0.2 to 1.5 THz, which operates in the polarizer-sample-rotating analyzer scheme. A BWO emitting intense and highly coherent radiation was used as light source. Two different samples, a low and a highly phosphorous-doped *n*-type Si substrate, were analyzed in order to illustrate properties of the new instrument. The measurements obtained from a highly phosphorous-doped Si substrate in the terahertz spectral range were found to be highly consistent with the best-model analysis obtained in the MIR spectral range.

Variable angle of incidence frequency domain terahertz ellipsometry in reflection configuration has been found to be a versatile tool for the determination of low free charge-carrier concentrations in semiconductors. The terahertz ellipsometry spectra of a low doped, double-side polished Si substrate show Fabry–Pérot oscillations which are damped toward lower frequencies. The quantitative analysis unambiguously provides the free electron concentration in silicon as low as $7.7\times10^{14}\,\mathrm{cm}^{-3}$ which corresponds to a plasma frequency of 0.14 THz and a mobility of $1617\pm80\,\mathrm{cm}^2/(\mathrm{V\,s})$. Terahertz ellipsometry is envisioned as noncontact, nondestructive investigation technique for accurate analysis of low-density free charge-carrier properties in semiconductor research and industry.

ACKNOWLEDGMENTS

The authors would like to acknowledge financial support from the Army Research Office (D. Woolard, Contract No. W911NF-09-C-0097), the National Science Foundation (Award Nos. 0922937 and 0907475) and NSF MRSEC QSPIN at UNL (DMR-0820521).

[1] P. Siegel, *Terahertz Sensing Technology: Electronic Devices and Advanced Systems Technology* (World Scientific, Singapore, 2003), pp. 1–44.
[2] D. Mittelman, *Sensing with Terahertz Radiation* (Springer, New York, 2004).
[3] D. Woolard, E. Brown, M. Kemp, and M. Pepper, Proc. IEEE **93**, 1722 (2005).
[4] M. Abo-Bakr, J. Feikes, K. Holldack, P. Kuske, W. B. Peatman, U. Schade, G. Wüstefeld, and H.-W. Hübers, Phys. Rev. Lett. **90**, 094801 (2003).
[5] F. Floreani, H. W. Koops, and W. Elsäßer, Nucl. Instrum. Methods Phys. Res. A **483**, 488 (2002).
[6] R. Köhler, A. Tredicucci, F. Beltram, H. E. Beere, E. H. Linfield, A. G. Davies, D. A. Ritchie, R. C. Iotti, and F. Rossi, Nature (London) **417**, 156 (2002).
[7] B. Ferguson and X. Zhang, Nature Mater. **1**, 26 (2002).
[8] S. E. Korbly, A. S. Kesar, J. R. Sirigiri, and R. J. Temkin, Phys. Rev. Lett. **94**, 054803 (2005).
[9] M. Tonouchi, Nat. Photonics **1**, 97 (2007).
[10] G. P. Williams, Rep. Prog. Phys. **69**, 301 (2006).
[11] J. S. Melinger, S. S. Harsha, N. Laman, and D. Grischkowsky, J. Opt. Soc. Am. B **26**, A79 (2009).
[12] H.-T. Chen, J. F. O'Hara, A. K. Azad, A. J. Taylor, R. D. Averitt, D. B. Shrekenhamer, and W. J. Padilla, Nat. Photonics **2**, 295 (2008).
[13] S. Zhang, Y.-S. Park, J. Li, X. Lu, W. Zhang, and X. Zhang, Phys. Rev. Lett. **102**, 023901 (2009).
[14] H. Němec, P. Kužel, F. Kadlec, C. Kadlec, R. Yahiaoui, and P. Mounaix, Phys. Rev. B **79**, 241108 (2009).
[15] M. Schubert, *Infrared Ellipsometry on Semiconductor Layer Structures: Phonons, Plasmons, and Polaritons*, Springer Tracts in Modern Physics, Vol. 209 (Springer, Berlin, 2004).
[16] H. Fujiwara, *Spectroscopic Ellipsometry* (Wiley, New York, 2007).
[17] D. E. Aspnes and A. A. Studna, Appl. Opt. **14**, 1131 (1975).
[18] R. W. Collins, Rev. Sci. Instrum. **61**, 2029 (1990).
[19] D. E. Aspnes, in *Handbook of Optical Constants of Solids*, edited by E. Palik (Academic, New York, 1998).
[20] J. Lee, P. Rovira, I. An, and R. Collins, Rev. Sci. Instrum. **69**, 1800 (1998).
[21] T. Nagashima and M. Hangyo, Appl. Phys. Lett. **79**, 3917 (2001).
[22] Y. Ino, R. Shimano, Y. Svirko, and M. Kuwata-Gonokami, Phys. Rev. B **70**, 155101 (2004).
[23] T. Hofmann, U. Schade, K. C. Agarwal, B. Daniel, C. Klingshirn, M. Hetterich, C. M. Herzinger, and M. Schubert, Appl. Phys. Lett. **88**, 042105 (2006).
[24] T. Hofmann, U. Schade, W. Eberhardt, C. M. Herzinger, P. Esquinazi, and M. Schubert, Rev. Sci. Instrum. **77**, 063902 (2006).
[25] T. Hofmann, C. M. Herzinger, T. E. Tiwald, J. A. Woollam, and M. Schubert, Appl. Phys. Lett. **95**, 032102 (2009).
[26] N. Matsumoto, T. Fujii, K. Kageyama, H. Takagi, T. Nagashima, and M. Hangyo, Jpn. J. Appl. Phys. **48**, 09KC11 (2009).
[27] P. Drude, Ann. Phys. **34**, 489 (1888).
[28] *Handbook of Ellipsometry*, edited by H. G. Thompkins and E. A. Irene (William Andrew, Norwich, 2004).
[29] R. M. Azzam and N. M. Bashara, *Ellipsometry and Polarized Light* (North-Holland, Amsterdam, 1984).
[30] All equations (wavelength, polarization, and angle-of-incidence dependencies) governing the boundary conditions of a given sample relating ρ (or subsequent definitions thereof) with the intrinsic polarizability functions and structure (symmetry, geometry, etc.) are left out in this communication. The interested reader is referred to existing literature, e.g., Refs. 15, 29, and 47–49.
[31] A. Röseler, *Infrared Spectroscopic Ellipsometry* (Akademie-Verlag, Berlin, 1990).
[32] E. Hecht, *Optics* (Addison-Wesley, Reading, 1987).
[33] Sample, mirrors, rotators, optical devices within the light path, and any combinations thereof.
[34] G. E. Jellison and F. Modine, Appl. Opt. **36**, 8184 (1997).
[35] G. E. Jellison and F. A. Modine, Appl. Opt. **36**, 8190 (1997).
[36] G. E. Jellison, in *Handbook of Ellipsometry*, edited by H. G. Thompkins and E. A. Irene (William Andrew, Norwich, 2004).
[37] C. Chen, I. An, and R. W. Collins, Phys. Rev. Lett. **90**, 217402 (2003).

[38] C. Brosseau, *Fundamentals of Polarized Light: A Statistical Optics Approach* (Wiley, New York, 1998).
[39] This set lacks the light beam's absolute intensity and the light beam's absolute phase information contained within the Jones matrix. For acquisition of generalized ellipsometry parameters from anisotropic samples, see Refs. 29, 50, and 51. Note that the choice of diagonal elements of the Jones matrix for normalization was convenient but arbitrary (Ref. 50).
[40] C. M. Herzinger, H. Yao, P. G. Snyder, F. G. Celii, Y.-C. Kao, B. Ohs, and J. A. Woollam, J. Appl. Phys. **77**, 4677 (1995).
[41] C. M. Herzinger, B. Johs, W. A. McGahan, and W. P. J. A. Woollam, J. Appl. Phys. **83**, 3323 (1998).
[42] C. Pidgeon, in *Handbook on Semiconductors*, edited by M. Balkanski (North-Holland, Amsterdam, 1980).
[43] C. Herzinger, S. Green, and B. Johs, U.S. Patent No. 6,795,184 (21 September 2004).
[44] B. Johs, Thin Solid Films **234**, 395 (1993).
[45] C. T. Kirk, Phys. Rev. B **38**, 1255 (1988).
[46] M. van Exter and D. Grischkowsky, Appl. Phys. Lett. **56**, 1694 (1990).
[47] W. S. Weiglhofer and A. Lakhtakia, *Introduction to Complex Mediums for Optics and Electromagnetics* (SPIE, Bellingham, 2003).
[48] P. Yeh, *Optical Waves in Layered Media* (Wiley, New York, 1988).
[49] M. Mansuripur, *The Physical Principles of Magneto-Optical Recording* (University Press, Cambridge, 1995).
[50] M. Schubert, in *Handbook of Ellipsometry*, edited by H. G. Thompkins and E. A. Irene (William Andrew, Norwich, 2004).
[51] M. Schubert, in *Introduction to Complex Mediums for Optics and Electromagnetics*, edited by W. S. Weiglhofer and A. Lakhtakia (SPIE, Bellingham, 2004), pp. 677–710.